ON WAVE-DRIVEN "SHINGLE" BEACH DYNAMICS IN A TABLE-TOP HELE-SHAW CELL

O. Bokhove[1], A.J. van der Horn[2], D. van der Meer[3], A.R. Thornton[4], W. Zweers[5]

The primary evolution of beaches by wave action takes place during storms. Beach evolution by non-linear breaking waves is 3D, multi-scale, and involves particle-wave interactions. We will show how a novel, three-phase extension to the classic "Hele-Shaw" laboratory experiment is designed to create beach morphologies with breaking waves in a quasi-2D setting. Idealized beaches emerge in tens of minutes due to several types of breaking waves, with about 1s periods. The thin Hele-Shaw cell simplifies the inherent complexity of three-phase dynamics by reducing the turbulence. Given the interest in the Hele-Shaw table-top demonstrations at ICCE2014, we will also discuss how different versions of the Hele-Shaw cell have been constructed. Construction can be inexpensive thus yielding an accessible and flexible coastal engineering demonstration as well as research tool. Beach evolution is sufficiently fast and can start very far from equilibrium, allowing an unusually large dynamical range to be investigated.

Keywords: shingle beaches, wave breaking, table-top realization, Hele-Shaw cell

1. INTRODUCTION

In recent years, there has been a fair amount of numerical modelling of detailed surf-zone dynamics with and without coupling to sediment and bed evolution at beaches. In the end all these numerical models require dispersed multi-phase modelling through some kind of averaging, either to deal with the fine-scale mixture of air and water bubbles and droplets during wave breaking (e.g., *Lachaume et al.* (2003); *Helluy et al.* (2005); *Dumbser* (2011)), or the three-phase mixture of air, water and (sand or shingle) particles (e.g., *Calantoni et al.* (2006) and *Bakhtyar et al.* (2012); *Deen et al.* (2012)). This detailed modelling forms an extension to the much more common and operational depth- and wave-averaged surf-zone morphodynamic models such as used, e.g., in *Soulsby* (1997); *Roelvink et al.* (2009); *Garnier et al.* (2010) and *McCall et al.* (2010). Most of this detailed numerical modelling is done in a vertical plane, in two dimensions, because in general the dynamics in a vertical plane is considered to be a useful test environment. This numerical modelling work in two dimensions is of academic character (including our own, e.g., *Gagarina et al.* (2013)) and cannot provide a realistic prediction of surf-zone dynamics, because wave breaking and particle transport are inherently three dimensional, especially on smaller scales.

To alleviate this shortcoming, we envision two alternative approaches. Firstly, instead of taking a vertical plane, we take a three-dimensional yet thin slice-of-beach as domain, such that the particle dynamics remain three dimensional. The computational effort is then still reduced considerably because the domain is so thin, and a periodic boundary condition can be used along the shore. Secondly, using such a slice instead of a fully two-dimensional domain opens the possibility to realize it within an experimental setting. The joint motion of liquid and particles can then be studied within the narrow space between two parallel plates. Waves are generated or enter the domain at one end and the particle beach lies at the other end, whereas the top is open (see Fig. 1).

Hele-Shaw flow concerns flow between two parallel plates seperated by a small gap, in which the viscous or Stokes flow profile is determined by the leading order balance between the viscous friction due to the proximity of the plates and the driving pressure gradient in the plane of the plates. That results in a predominantly parabolic or Poiseuille flow velocity profile between the plates. When one places objects between the glass plates, the streamlines of the laminar flow around these objects can be visualized (*Hele-Shaw*, 1898). The width of the gap can be optimized such that in the plane of the cell, inertial effects become more or less important. When inertial effects become larger, larger deviations from the Poiseuille profile emerge. We extended Hele-Shaw's original laboratory experiment (*Hele-Shaw*, 1898) into a three-phase version within the vertical plane with air, water and particles. It allows the study of beach dynamics in a tank with a narrow gap, which is in the most extreme case just over one diameter to a few particle diameters wide. In contrast to the numerical models in the vertical plane, particle dynamics in the Hele-Shaw set-up remain three-dimensional (*Bokhove et al.*, 2010).

The advantages of this set-up for studying beach dynamics are as follows:

---

[1]School of Mathematics, University of Leeds, LS2 9JT, Leeds, U.K.
[2]Department of Physics, University of Twente, Enschede, 7500 AE, The Netherlands
[3]Department of Physics, University of Twente, Enschede, 7500 AE, The Netherlands
[4]Department of Applied Mathematics/Mechanical Engineering, University of Twente, 7500 AE, Enschede, The Netherlands
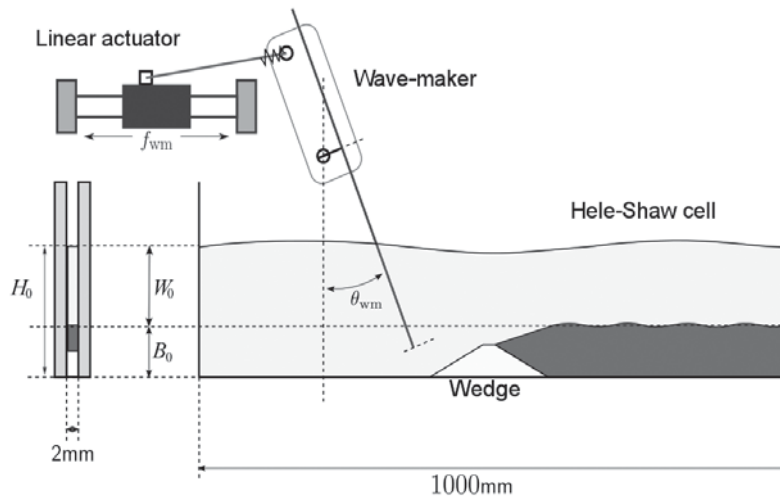[5]FabLab, Saxion College, Enschede, 7513 AB, The Netherlands

Figure 1: Schematic of Hele-Shaw cell. Wedge, waterline, particle bottom, and wave-maker are shown. Parameters are initial water depth $W_0 = H_0 - B_0 = (10, 30, 50, 70) \pm 3$ mm, bed level $B_0 = (20, 50, 80) \pm 2$ mm at rest, and wave-maker frequency $f_{wm} = (0.4, 0.7, 1.0, 1.3)$ Hz with angle θ_{wm}.

- the dynamics of the two fluids, air and water, and the particles is fully visible, since the "gravel" particles of the "shingle" beach are not blocking the view;

- turbulence has been greatly reduced or even removed so one can focus on wave-induced bed transport including breaking waves;

- the experimental data have great potential for the validation of existing and new predictive models;

- the time scales of the beach dynamics are much shorter than at natural beaches or in large wave flumes, thus permitting a study of the dynamics very far from quasi-equilibrium; and,

- the (portable and affordable) set-up fits on a table-top such that it can also serve as an accessible teaching and a pubic demonstration tool.

Three possible disadvantages are in order of importance: the hydrodynamic damping due to the proximity of the glass plates, the effect of surface tension, and contact-line damping at the glass plates. The goals of our study then become the following:

- to summarize the mathematics of the design of the Hele-Shaw beach set-up addressing the aforementioned disadvantages,

- to study the dynamics obtained in this table-top experiment,

- to report how we contructed several Hele-Shaw cells for the benefit of further development and use, and

- to discuss its potential for improving numerical multiphase models for surf-zone morphodynamics.

These goals are matched by the following outline. In Section 2, the mathematical design is summarized. Subsequently, we show in Sections 3 and 4 that all types of wave breaking can occur during the bed evolution such that a variety of interesting quasi-steady beach profiles emerge. Given the increased damping due to the proximity of the glass plates, offset in part by large wave forcing, we show that the Gamma Alumina particles used in our beach experiments, behave more like shingle than sand beaches (*Short*, 2000; *Powell*, 1990). In Section 5, we highlight prominent features and differences in a comparison of the three

table-top realizations constructed hitherto. Finally, we conclude in Section 6. The work in this article runs partially in parallel with our previous work (*Thornton et al.*, 2014), but concerns different data sets, which shows that the experimental results are robust. In addition, a comparison between different realizations of the Hele-Shaw cell is made.

2. MATHEMATICAL DESIGN OF HELE-SHAW BEACH

The simplified table-top dynamic beach with breaking waves in Fig. 1 is a so-called Hele-Shaw cell. It is an extension with the three phases air, water and particles of the original (liquid-filled) cell developed by Hele-Shaw (*Hele-Shaw* (1898); *Lamb* (1993)). It consists of two glass plates put in the vertical plane with bottom and sides closed and an open top (see Fig. 1). The design of our Hele-Shaw beach experiment was based on mathematical analysis of approximate models for the hydrodynamics for a fixed bed. Even though we are interested in bed erosion and creation by breaking waves, the case with a fixed bed allowed us to calculate the optimal gap width between the two glass plates before the experiment was built. To obtain an estimate of this optimal gap width, we will simplify the hydrodynamics and summarize a validation of the resulting two-dimensional "Navier-Stokes" equations against damped wave experiments, before highlighting the predictions of a shallow-water model of wave breaking on a fixed sloping beach.

A narrow gap width between the glass plates, just over one particle, is desirable to enhance the visualization and limit the dynamics to be nearly two-dimensional. At the same time, this gap needs to be wide enough to allow for nonlinear breaking waves and beach formation. In the classic Hele-Shaw case, the parabolic flow profile in the vertical plane (e.g., *Batchelor* (1967); *Wilson and Duffy* (1998)) is

$$(u, w) = \frac{3}{2}(\bar{u}, \bar{w})(l^2 - y^2)/l^2 \tag{1}$$

with $u = u(x, y, z, t)$ and $w = w(x, y, z, t)$ the velocity components in the horizontal, x, and vertical, z, directions, lateral direction y, gap width $2l$ and the laterally averaged mean velocities $\bar{u} = \bar{u}(x, z, t)$ and $\bar{w} = \bar{w}(x, z, t)$, and time t. Under the approximation that the local flow profile is parabolic in the lateral direction, we can substitute (1) into the three-dimensional Navier-Stokes equations for the hydrodynamics of water and average these across the gap. Given the anisotropy in the length and velocity scales along and normal to the vertical plane, the viscous balance across the gap is assumed to be dominant. An approximation is then made in which slow variations in the vertical plane on scales larger than the gap width are still permitted. After averaging and neglecting Reynolds-stress terms, the resulting two-dimensional Euler or "Navier-Stokes" equations with linear momentum damping become

$$\frac{\partial \bar{u}}{\partial t} + \beta \bar{u} \frac{\partial \bar{u}}{\partial x} + \beta \bar{w} \frac{\partial \bar{u}}{\partial z} = -\frac{1}{\rho} \frac{\partial p}{\partial x} - \frac{3\nu \bar{u}}{l^2}, \tag{2a}$$

$$\frac{\partial \bar{w}}{\partial t} + \beta \bar{u} \frac{\partial \bar{w}}{\partial x} + \beta \bar{w} \frac{\partial \bar{w}}{\partial z} = -\frac{1}{\rho} \frac{\partial p}{\partial z} - \frac{3\nu \bar{w}}{l^2} - g, \tag{2b}$$

$$\frac{\partial \bar{u}}{\partial x} + \frac{\partial \bar{w}}{\partial z} = 0, \tag{2c}$$

in which ν is the viscosity of water, g the acceleration of gravity, $p = p(x, z, t)$ the pressure, ρ the constant density of water, and $\beta = 6/5$ a scaling factor originating from the width-averaging mentioned. The first two equations are the momentum equations in the x– and z–directions, and the last equation expresses that this width-averaged velocity in the vertical plane is incompressible. Higher-order contributions beyond the lateral flow profile (1) are ignored in (2), which especially concerns omissions in the three-dimensional boundary layers near the free surface, side walls and near particles. In contrast to classical Hele-Shaw flow (*Hele-Shaw*, 1898), by design we aim to include inertial effects in the vertical plane, with (weak) deviations from the parabolic profile, cf. investigations in other Hele-Shaw cells on Faraday free surface waves (*Rajchenbach et al.*, 2011) or Kelvin-Helmholtz instability (*Plouraboué and Hinch*, 2002). Nevertheless, for the flow in the bulk away from boundaries, these linear damping terms in the momentum equations of (2) are reasonable, as we will discuss next.

Validity of Linear Momentum Damping

To assess the validity of the hydrodynamical model (2), we compared water wave simulations based on (2) *a posteriori* with simple damped wave experiments in our Hele-Shaw cell without particles. We

substitute $(\bar{u}, \bar{w}) = (\partial\phi/\partial x, \partial\phi/\partial z)$ with velocity potentrial $\phi = \phi(x, z, t)$ into (2) in a domain with a free surface and fixed bottom as well as side walls, to obtain the potential flow equations for water wave motion but with an additional linear damping term. To simplify the presentation, we set $\beta = 1$ hereafter, but this does not change the argument below regarding the potential energy. The resulting system of water wave equations can be derived succinctly from the following variational principle

$$
\begin{aligned}
0 &= \delta \int_0^T \left(\int_0^L \phi_s \frac{\partial h}{\partial t} \mathrm{d}x - (P(t) + K(t)) \right) e^{3\nu t/l^2} \mathrm{d}t \\
&\equiv \delta \int_0^T \left(\int_0^L \phi_s \frac{\partial h}{\partial t} - \frac{1}{2}g(h - H)^2 \mathrm{d}x - \int_0^L \int_0^h \frac{1}{2}|\nabla\phi|^2 \mathrm{d}x\,\mathrm{d}z \right) e^{3\nu t/l^2} \mathrm{d}t
\end{aligned}
\tag{3}
$$

with water depth $h = h(x, t)$, the potential at the free surface $\phi_s = \phi_s(x, t)$, mean still water depth H, kinetic energy $K(t)$, potential energy $P(t)$, suitable boundary and end-point conditions for a tank of length L and with a final time T. Miles' classic variational principle for potential flow water waves (*Miles*, 1977) arises from (3) in the inviscid limit for $\nu = 0$, while our damped case in (3) includes the additional factor $\exp(3\nu t/l^2)$. The latter factor is the inverse of the integrating factor due to the linear momentum damping in (2). (Note that the solution to two of the terms in (2), i.e., $\partial\bar{u}/\partial t = -3\nu\bar{u}/l^2$ is $\bar{u} = \bar{u}_0 \exp(-3\nu t/l^2)$.) The consequence of (3) is that in the damped case without forcing it is more revealing to plot the modified potential energy (per unit width), $\rho P(t) \exp(3\nu t/l^2)$ rather than $\rho P(t)$ itself.
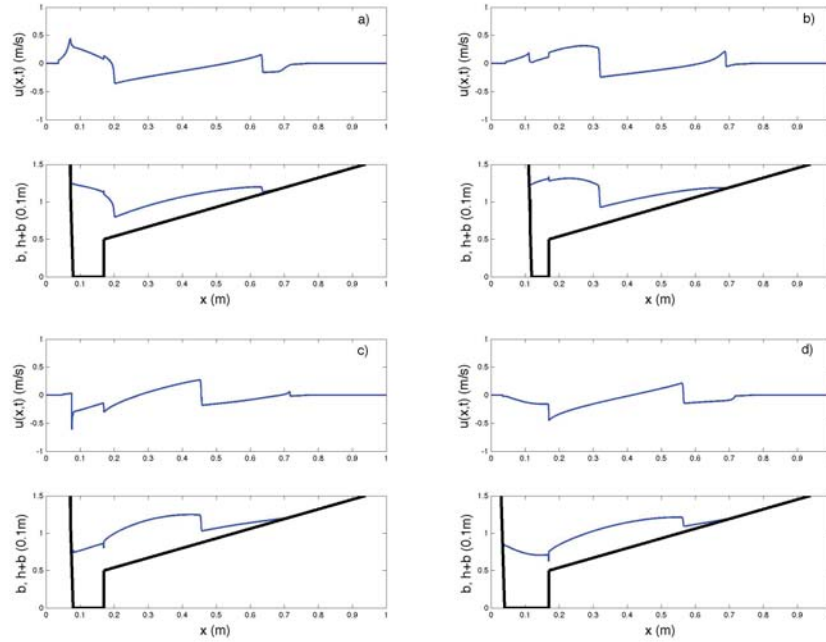

Figure 2: **To determine the threshold gap width** $2l$**, simulations of shallow-water simulations were performed in the model (4) for** $\gamma = 1$**: snapshots of depth-averaged velocity** $u = \bar{u}(x, t)$**, topography** $b(x, t)$ **(black, fat line) and free surface** $h(x, t) + b(x, t)$ **(blue, normal line), for** $2l = 1.8$mm **and wave-maker frequency** 1.2Hz**. The wave-maker is modelled as a steep, moving wall with fixed** $\partial_x b(x, t) < 0$ **(seen on the left), while the topography** $b(x)$ **on the right is fixed. a)** $t = 3.25T$**, b)** $t = 3.5T$**, c)** $t = 3.75T$**, and d)** $t = 4.0T$ **with period** $T = 1$s**. A similar yet different simulation is found in** *Thornton et al.* **(2014).**

In *Thornton et al.* (2014), a comparison between the potential flow model arising from (3) and a damped wave-sloshing experiment in the rectangular Hele-Shaw cell with fixed walls shows that experimental data and simulations compare reasonably well, for about one to one-and-a-half long-wave period. Hence, we have shown that for driven flows on scales much larger than the gap width, the linear momentum damping in (2) and (3) is a good leading-order model approximation because new waves keep coming in. The modelling of the fine-structure in breaking waves may require resolution of three-dimensional free-surface boundary

layers (cf. *Vega* (2001) in a related yet different free-surface problem on Faraday waves), the inclusion of other flow profiles, and damping of the contact line (*Vella and Mahadevan*, 2005) at the water-air-glass interface.
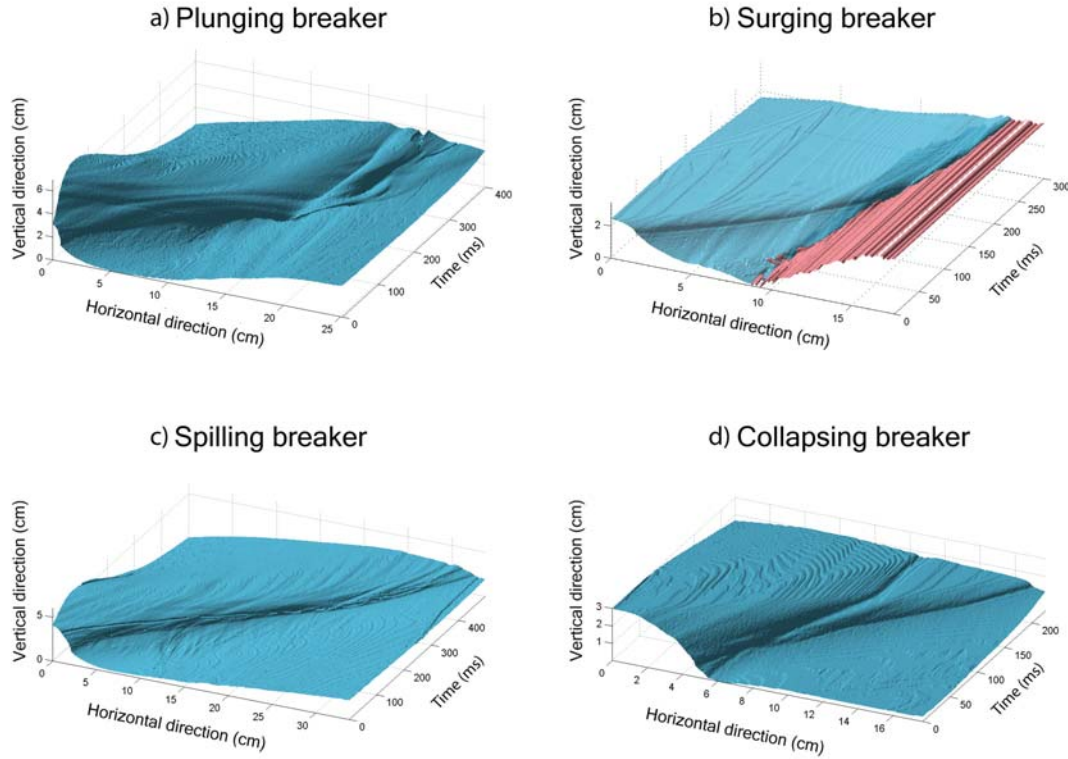

Figure 3: Space-time plots of breaking waves. The water surface (blue) and bed (red) of measured a) plunging, b) surging, c) spilling and d) collapsing breakers.

The final design step was to derive a depth-avaraged shallow-water model by averaging (2) over the depth and using the corresponding kinematic condition at the free surface (extending the classic derivation in, e.g., *Pedlosky* (1987)). The resulting shallow-water equations with linear momentum damping (*Thornton et al.*, 2014) are as follows

$$\frac{\partial(h\bar{\bar{u}})}{\partial t} + \frac{\partial}{\partial x}(\gamma h\bar{\bar{u}}^2 + gh^2/2) = -gh\partial b/\partial x + (\gamma-1)\bar{\bar{u}}\frac{\partial(h\bar{\bar{u}})}{\partial x} - 3\nu h\bar{\bar{u}}/l^2 \quad \text{and} \quad \frac{\partial h}{\partial t} + \frac{\partial(h\bar{\bar{u}})}{\partial x} = 0 \qquad (4a)$$

with the water depth $h = h(x,t)$, depth- and width-averaged horizontal velocity $\bar{\bar{u}} = \bar{\bar{u}}(x,t)$, bottom topography $b = b(x,t)$ as function of the horizontal coordinate x and time t. These are augmented with the usual hydaulic bore relations (*Lamb*, 1993) such that the solutions remain single-valued except at isolated locations where wave breaking processes are modelled as discontinuities in the water depth and velocity. We performed various numerical simulations of these depth-averaged shallow water equations with linear momentum damping for $\beta = 1$ and different values of the gap width $2l$, as well as different wave-maker amplitudes and frequencies around 1 Hz. A typical breaking wave in the form of a hydraulic bore was found to survive the damping and travel across this fixed sloping beach of circa 0.5m length in the corresponding numerical shallow water model for gap widths $2l > 1.5$ mm and frequencies of about 0.5–1.3 Hz (*Thornton et al.*, 2014). Sample profiles of $h(x,t)$ and $\bar{\bar{u}}(x,t)$ of one simulation are shown in Fig. 2. For smaller gap widths and other frequencies, the bore would dampen out before reaching the water line. Hence, we chose the Hele-Shaw cell to have a gap width of $2l = 2$ mm given available Gamma Alumina particles with diameter $d = 1.75 \pm 0.05$ mm and effective density 2.08 ± 0.2g/cm^3 with water-filled pores. We note that

Lee et al. (2007) considered one particle settling in a Hele-Shaw cell, and observed quasi-two-dimensional behaviour for gap widths $2l < 1.05d$, and three-dimensional behaviour for $2l > 1.1d$. With our choice of $2l = 2$ mm and $d = 1.75 \pm 0.05$ mm, we are in a quasi-three-dimensional regime of particle settling.
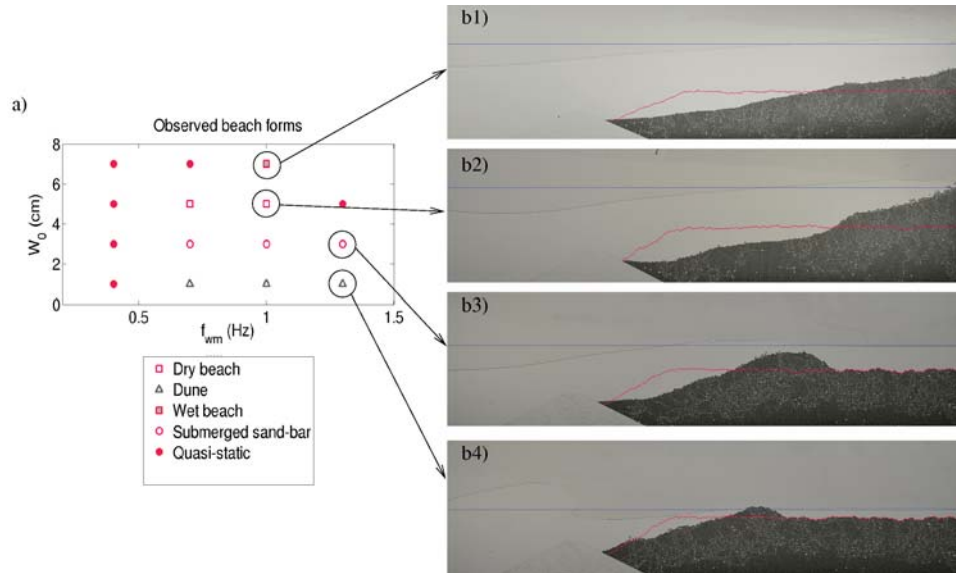

Figure 4: Phase diagram of beach morphologies. a) States in the parameter plane of initial water depth $W_0 = H_0 - B_0$ and wave frequency f_{wm}, for an initial bed level of $B_0 = 8$ cm. (For $B_0 = 2$ and 5 cm the state is quasi-static, except for $f_{wm} = 1$ Hz, $B_0 = 5$ cm and $W_0 = 5$ cm, for which a sand bar developed.) b) Initial water levels and bed heights (blue and red lines, respectively) and final bed height for a: b1) wet beach, b2) dry beach, b3) sand bar, and b4) berm/dune.

3. WAVE BREAKING

Since we are interested in bed profiles emerging under breaking waves, we first report which types of wave breaking occur in the Hele-Shaw cell. We found all types of wave breaking over dynamic beaches, described in *Peregrine* (1983), including spilling, plunging, collapsing and surging breakers. The water was dyed red to enhance the contrast and facilitate analysis of the measurements, obtained by a high speed Photron SA2 camera at 1000fps. Space-time renderings of the four wave types are shown in Fig. 3, and discussed in turn. In a plunging breaker, the wave front overturns and a prominent jet falls at the base of the wave causing a large jet, Fig. 3a. We observe two bubbles caught during overturning. For a surging breaker, a significant disturbance and vertical face in an otherwise smooth profile occurs only near the moving shoreline, Fig. 3b. In a spilling breaker, whitish water at the wave crest spills down the front face sometimes with the projection of a small jet, Fig. 3c. The grooves indicate the presence of (pre-existing) bubbles. In a collapsing breaker, the lower portion of the wave's front face overturns and then behaves like a plunging breaker, Fig. 3d, where the lower portion of the wave is seen to shoot forward after circa 100ms, and to separate from the top part of the wave. In the Hele-Shaw set-up these wave types are small-scale versions smoothed by surface tension, when compared to violent three-dimensional breakers at beaches.

In a companion study (*Thornton et al.*, 2014), we analyze the Irribarren number $\tan \alpha / \sqrt{H_b/L_b}$ of these waves with slope angle α, breaker wave height H_b and wave length L_b (*Battjes*, 1974). Even for long waves L_b is based on the linear deep water waves. While at natural beaches $I_b < 0.4, 0.4 < I_b < 2.0, 2.0 < I_b < 3.3, I_b > 3.3$ for spilling, plunging, collapsing and surging breakers, respectively, our preliminary measurements in the first Hele-Shaw cell yield $I_b = 0.8, 1.6, 1.7,$ and 1.9, respectively. These types of wave breaking emerged during various stages of bed evolution into sand bars, beaches or berms, considered next in detail.
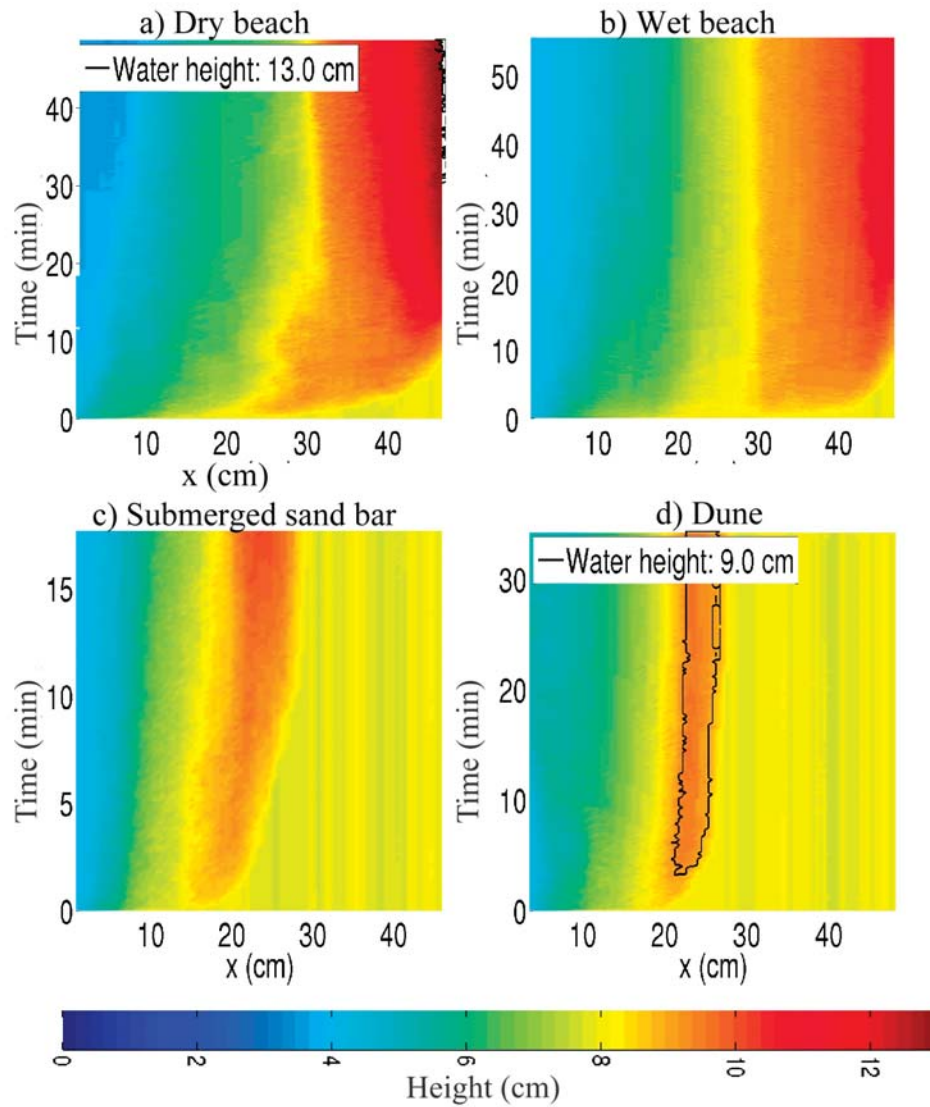
Figure 5: Bed heights in space-time. Time-space diagrams of bed height versus spatial coordinate *x* for a) dry and b) wet beaches (boundary maxima), and c) a submerged sand bar and d) a berm/dune (interior maxima). When dry land emerges the initial water level (black line) is indicated, in d) but also in a)!

4. QUASI-STEADY BEACH MORPHOLOGIES

Time-dependent beach morphologies form on a time scale of minutes to hours, forced by waves that occur on a typical time scale of one second. We undertook a parameter study (Van der Horn, 2012) of beach formation by the action of (breaking) waves in which we varied the initial water depth $W_0 = (10, 30, 50, 70)$ mm and bed level $B_0 = (20, 50, 80)$ mm at rest, before turning on the wave-maker in a monochromatic frequency range of $(0.4, 0.7, 1.0, 1.3)$ Hz (recall Fig. 1). The state of the bed was captured every 10s with a Nikon D5100 camera. Depending on the parameters, several quasi-steady beach profiles were observed to develop after 10 to 30 minutes.

These profiles are classified based on their physical nature using the mathematical bed profile $b = b(x)$, with $b \approx B_0$ initially. When this bed profile $b(x)$ has an interior maximum, its maximum is either submerged ("sand bar"), or dry on top on its onshore side ("berm-dune or beach-dune"). When this bed profile $b(x)$ has a boundary maximum, it is either wet or dry ('wet or dry beach'). A berm or dune emerges when water is found at both sides of a berm. A beach-dune is a berm near the right wall, also with an interior maximum bed height away from the boundary. A submerged sand bar arises when a "significant" amount of sediment area transport, more than 10cm^2 over the duration of the experiment, is taking place with an interior, wet maximum of the bed height, and when none of the above definitions hold. Finally, in the quasi-static state hardly any sediment area transport is taking place (less than 10cm^2 and no parts fall dry). Four of these states are displayed in Fig. 4, displaying both initial and final states, together with a phase diagram for the case $B_0 = 80$ mm. Space-time plots of the bed height evolution from a nearly flat submerged bed to the dune, dry beach, wet beach or sand bar are given in Fig. 5, and range from 20 to 60 minutes. It is clear in the phase diagram in Fig. 4 that the states evolve smoothly from one to the other. Furthermore, the activity of the wave is less efficacious when: the wave has already lost its energy due to its breaking over the wedge; the water is very shallow; the frequency is too high such that the viscous damping becomes too high; or, when the water is too deep such that particles do not get picked up. The wet beach state emerges when there are insufficient particles available to create a dry beach. Our beach profiles are remarkably similar to those in *Powell* (1990) for shingle beaches in a $42 \times 1.5 \times 1.4\text{m}^3$ wave tank, which in turn resemble natural shingle beaches. The difference is that our mean slope is with circa $1:3$ about two times steeper than the one in *Powell* (1990). In *Thornton et al.* (2014) other measurement series reveal similar results, confirming the robustness of our findings.
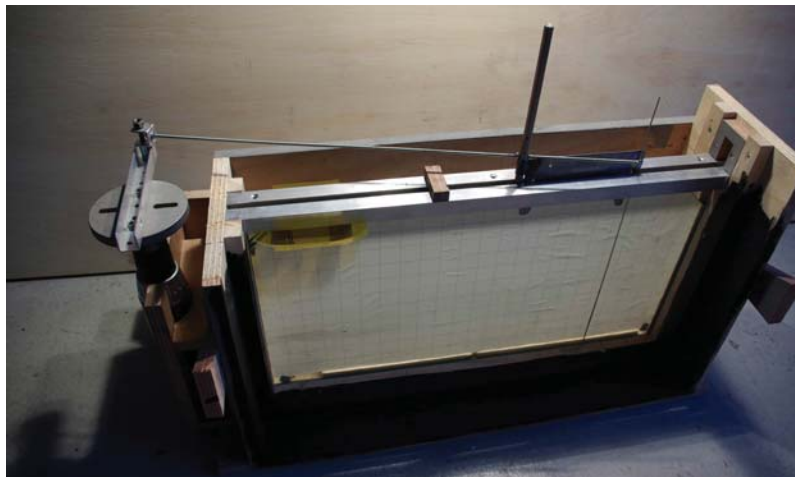

Figure 6: Photograph of the first Hele-Shaw cell without water and particles. It shows the straighforward wave-maker construction with the drill on the left, the transfer of rotational to translational motion, the wave-maker rod and background grid.

5. COMPARISON AND CONSTRUCTION OF THREE DIFFERENT SET-UPS

Hitherto, three different realizations have been constructed of the Hele-Shaw cell to study beach dynamics. The first one was build in January 2010 for a public demonstration at the Qua Art Qua Science event

"Fluid Fascinations" (*Bokhove et al.*, 2010). It featured as a dynamic and visual illustration of the beauty of fluid dynamics in the opening presentation. The motion of the intermittently breaking water line and the underlying particle movement in the live demonstration was instantaneously recorded on camera and projected on a large screen. The event concerned 13 artworks made by the artist Valerie Zwart, inspired by and based on fluid dynamical slides from the late Professor Howell Peregrine (Cooker, 2010)[6]. The mathematical design of the Hele-Shaw beach experiment and its construction were presented to highlight a shared fascination with fluid dynamics and coastal engineering (*Bokhove and Peregrine*, 1998). The dimensions of this cell are $0.6 \times 0.002 \times 0.3 \text{m}^3$. The glass plates are spaced 2mm apart and seperated by two hard-plastic spacers along the two vertical sides and flat bottom. Duct-Tape is used to seal the plates on these three sides. The entire construction is placed in a wooden frame. Wooden strips screwed tightly onto a wooden floorplate and side boards allowed one two squeeze the glass plates tightly against the plastic spacers. Due to the water pressure, the glass plates slightly widened at the open top, especially in the middle. With two small spacers and two small clamps this is minimized. Later a system of nuts and bolds was constructed to squeeze the glass plates together through multiple holes in two aluminum U-bars attached vertically to the wooden side boards, with their open sides facing another. The Gamma Alumina particles of diameter 1.75mm were used as "shingle" or "gravel". Wave motion is generated by an affordable and rechargeable drill, which rotating motion in the horizonal plane was transformed into linear motion along rails consisting of two aluminum U-bars, facing another, via an axel. Attached to a wagen rolling on four metal wheels in these two parallel U-bars is a vertical pin consisting of a welding rod, circular with a 1.5mm cross section. This rod pushes the fluid between the two glass plates spaced thus generating the wave motion. Via a wooden wedge on a string the drill speed is controlled, yielding a frequency of the wave motion around 1Hz. The rod traverses across about a third of the tank length (i.e. 0.2m) over nearly the entire water depth. Particles near the wave-maker rod can trouble its motion, and potentially cease it. A perched beach set-up is therefore used with a wedge keeping the beach section of particles in seperation from the flat-bottomed wave-maker section of the cell. The wedge is a quadrilateral in shape with a longer base face parallel to a shorter top face. A photograph of the dry set-up is shown in Fig. 6. Perched beaches are beaches where an underwater offshore rigid barrier, parallel to the shore and either manmade or natural, limits or prevents loss of onshore beach particles to the offshore side. It prevents the beach from disappearing. The wedge is made of an old creditcard, taped up to fit sufficiently well between the two glass plates, in such a way that it can still be removed with a pick (a welding rod with a hook a the end). A wooden suitcase on wheels was later build around the set-up to allow (transatlantic) transport of all equipment. The study of the Iribarren number of the four types of breaking waves in *Thornton et al.* (2014) is based on the study of early footage of beach formation and breaking waves in this first set-up from January 2010, recorded at 50fps. Disadvantages of this set-up are as follows:

- The sealing by Duct-Tape is prone to leaking.

- Cleaning of the tank to remove water and especially the particles is cumbersome. It is also a time-consuming task to take out the glass plates, clean and reassemble them again.

- The entire set-up weighs circa 23.5kg, which makes it less portable.

- The tank was too short, given the long section required for the wave maker motion, and only revealed similar bar, wet and dry beach formation, such as reported in Section 4, but no berm formation.

- The drill-operated wave motion can only be harmonic and needs to be adjusted by hand.

- Only perched beaches can be investigated due to the required wave-maker section devoid of particles.

The second version, built mainly by W.Z., included several improvements to permit more quantitative scientific research:

- A longer cell was used of dimensions $0.6 \times 0.002 \times 0.3 \text{m}^3$ and again set in a larger wooden frame.

- An inexpensive programmable wave-maker was made by using a disassembled printer and Arduino technology, see Fig. 7. A programmed harmonic wave turned out to become non-sinusoidal because the printer motor was not sufficiently strong. It was replaced by a strong but more expensive

---

[6]V.Z. and O.B. were given these slides by the School of Mathematics in Bristol, with permission from the Peregrine family.

Figure 7: The second, dry Hele-Shaw cell with the linear, programmable motor of a disassembled printer on the right, the black wedge in the middle, white particles, and the clamping system.

programmable stepping motor in combination with the inverted pendulum consisting of two welding rods displayed in Fig. 1, instead of two vertical welding rods. Programmed harmonic motion remained nearly harmonic, see Van der Horn (2012).

- The glass plates were sealed together permanently, and in one corner there was an in- and outlet valve with a hose, closed off during operation of the wave-maker. This facilitated cleaning. Leakage repairs were only occasionally required since the alcohol for cleaning the tank dissolved the sealing kit when the alcohol was not flushed out sufficiently quickly. Similar 2mm spacer and U-bar clamp techniques were used as in the first set-up.

- More attention was paid to screening and lighting such that high quality images were obtained, using photography for the bed evolution (at 10s intervals) and short-time footage for breaking waves (at 1000fps). Again, only perched beaches can be investigated due to the required wave-maker section devoid of particles. Given its increased weight and size, the second tank is less portable than the first, but still fits on a table-top.

The third version of the Hele-Shaw cell, built by W.Z., is the portable version demonstrated at ICCE2014 and at open days of the School of Mathematics, see Fig. 8. It contains of the following improvements:

- It has dimensions $0.7 \times 0.002 \times 0.2\text{m}^3$. The tank consists of two glass plates in a metal frame, held upright by two removeable metal stands at one side. The heavy, wooden frames in the two previous versions have therefore been removed. See Figs. 8 and 10.

- It has a drill-operated wave pump connected to two syringes (inner diameter circa 0.04m) acting as pistons in two vertical pipe sections attached to two hoses, one leading to the bottom corner of the tank, and one to a valve for the addition and removal of water and particles. See the sketch in Fig. 9. Smooth movement of the pistons requires vaseline to be used as a lubricant.

- When the hoses, wave pump, rechargeable drill and tank are disassembled, the entire kit fits in a large suitcase with room to spare for personal travel ware. This ensures portability.

- Particles can freely flow anywhere in the tank. The beaches developing are not perched beaches and as a consequence different quasi-equilibrium states were for the first time observed at the ICCE2014, relative to those observed before in the other wave tanks, as reported in Section 4 and *Thornton et al.* (2014). Beach evolution and cliff formation are elucidated in Figs. 10 and 11.

Figure 8: Photograph of the portable Hele-Shaw set-up on the left and with the lead author on the right. Photo courtesy: Jannette Frandsen at the ICCE2014.
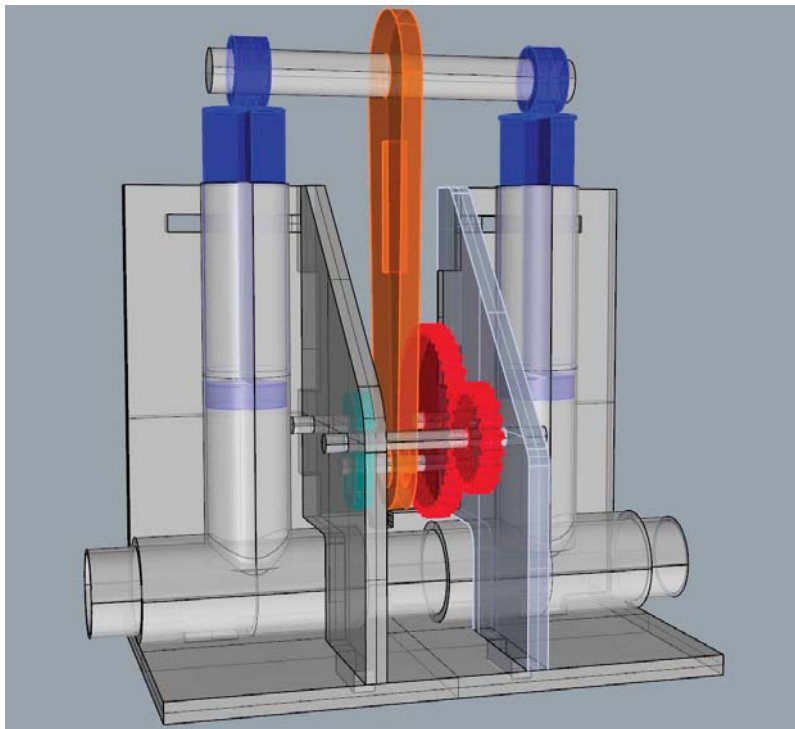

Figure 9: CAD rendering of the wave pump design is shown with the two syringe pistons and gear box.

- The building costs are relatively low, making the set-up generally affordable provided one has the hours available to construct it. This is an important point, stressed by several ICCE2014 participants through remarks like: "finally a wavetank that is affordable by researchers in all countries" [7]

Nonetheless, the portable version displayed at ICCE2014 requires the following improvements:

- Particles can flow back into the hose, even though this does not obstruct the operation, and the inflow of water in the bottom corner of the tank causes the bottom of the tank to become bare. We therefore aim to let the water flow into the tank at a higher level with a smoother inflow section, combined with a fine gauze to prevent the particles from flowing back into the hose.

- The wave pump design requires turning and greasing, and will be made more rigid. While the drill operates at sufficiently low speeds, the rechargeable battery lasts insufficiently long. Its speed is tuned using tie-wraps, which is less inflexible, causing a sudden splash of water at the start.

- It is still too heavy, circa 11kg, so a plexiglass or aluminum version with glass plates is in the making.
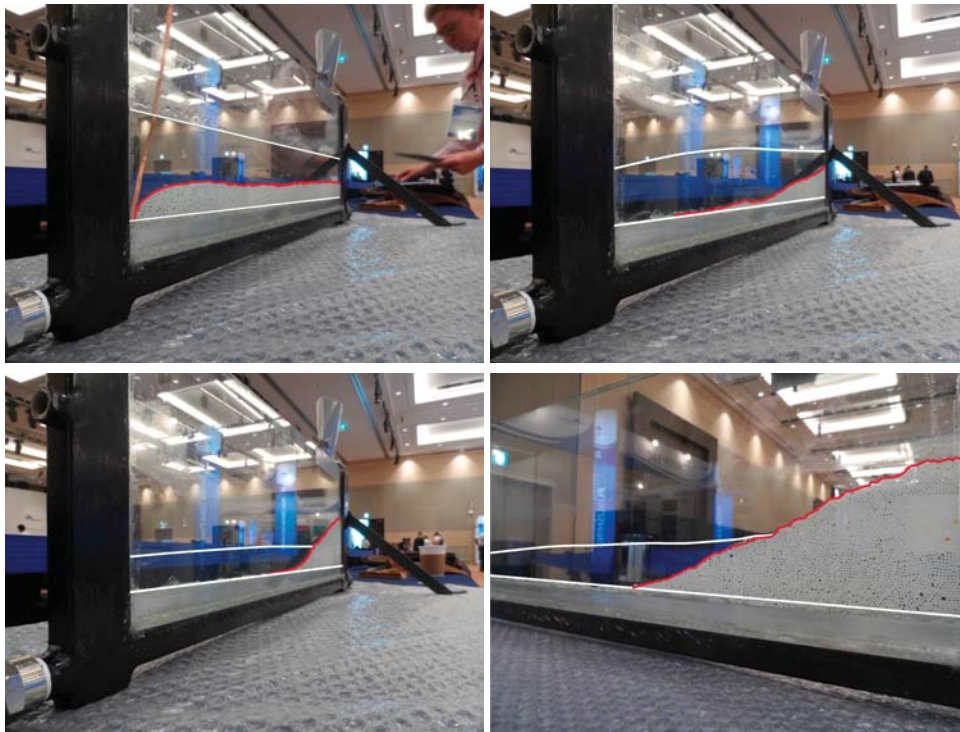

Figure 10: Starting from a flat layer of particles and using wave-maker motion operated at a fixed drill speed, a dry beach emerges after a few minutes (top left, top right, bottom left, bottom right). The height of the dry land is governed by the maximum wave height available to deposit a particle at the beach top. In the end, a quasi-equilibrium is reached after about 14min, given the finite amount of particles. Snapshots at $t = 10{:}24{:}18$, $10{:}26{:}19$, $10{:}32{:}01$, $10{:}32{:}16$hr. The waterline and bed profile have been enhanced. The inflow connection is seen at the bottom left corner of the first three images. In the top left image, a strip is holding back the particles during the levelling the tank. Movies of the beach formation can be found at the public facebook page "Resurging Flows" of O.B and W.Z.

---

[7]"Can I make a movie and photographs?" was a question posed several times during the demonstrations at ICCE2014, to which O.B.'s answer was: "Yes, please do but please refer to our articles".
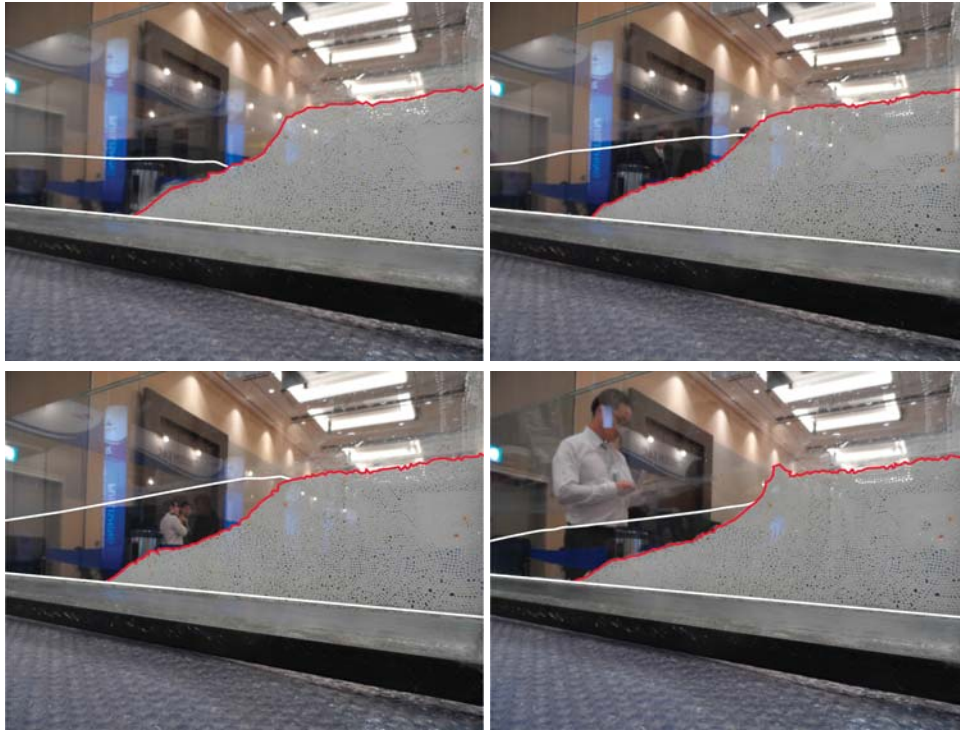
Figure 11: The flat beach top progresses offshore once its maximum height has been reached. Snapshots at t = 10:42:05, 10:54:16, 10:54:35, 10:59:50**hr. From the second last (bottom left) to last frame (bottom right) the wave frequency was raised, which increased the wave height thus leading to the formation of a localized, higher cliff.**

6. CONCLUSIONS AND DISCUSSION

We demonstrated the proof-of-concept of simplified beach dynamics caused by breaking waves in an adaptation of the table-top laboratory experiment by Hele-Shaw (*Hele-Shaw*, 1898) containing the three phases water, solid particles and air. A few simplified models of fluid dynamics were analysed to aid the design of our experiment, but we did not yet provide (numerical) predictions of observed wave and bed profiles.

A future goal is to validate aspects of mathematical and numerical models of beach and wave morphology against beach dynamics in this table-top slice-of-beach with wave breaking. The set-up investigated was not meant to closely mimic dynamics at natural beaches but the quasi-equilibrium bed profiles compare qualitatively surprisingly well with shingle beach experiments (*Powell*, 1990; *Williams et al.*, 2012). The bed profiles we found are, however, twice as steep. Turbulence is dampened significantly in our Hele-Shaw cell, which is a departure from reality at natural beaches or shingle beach experiments in large wave flumes. The Hele-Shaw set-up does, intentionally and by design, allow a focus on wave breaking and fluid-particle interactions without the need for turbulent closures, the latter which generally lead to numerical predictions that are smoothened (e.g., see *Bakhtyar et al.* (2012), their Fig. 2) to such an extent that the predictions tend to resemble our table-top free-surface measurements more closely than actual natural beach dynamics.

A key characteristic of our Hele-Shaw beach experiment is that particle, wave and water motions can be measured and analysed thoroughly in the entire domain. This may allow closure relations for fluid-particle interactions to be measured directly, a task that is usually reserved for numerical simulations. A combined numerical and experimental approach has the added benefit that the observed interactions are real, thus suffering neither from numerical errors nor closure problems.

The Hele-Shaw modelling environment for beach dynamics was designed to allow a complementary validation of new (*McCall et al.*, 2010; *Vega*, 2001; *Thornton et al.*, 2006; *Dumbser*, 2011) and existing forecasting models (*Operational forecast models*, 2014). In addition, it permits various extensions: one can

think of using different initial bed and substrate slopes (*Short*, 2000), particles of varying size and density, in order to mimic dynamics ranging from sand to shingle beaches (*Short* (2000); *Powell* (1990)), wider gap widths to systematically increase the influence of turbulence, more complex and different wave-maker motions, and changing water levels (e.g, mimicing tides). We aim to consider these extensions in the future and hope our work will inspire others.

Finally, an overview was given of the construction and operation of three different realizations of the Hele-Shaw set-up. One of these is a portable version, demonstrated at the ICCE2014, showing its potential as an affordable wave tank to illustrate and investigate fundamental aspects of beach formation and destruction by (breaking) waves in the classroom, in a small-scale research setting, and to the general public.

References

Bakhtyar, R., Barry, D.A., and Kees, C.E. 2012. Numerical experiments on breaking waves on contrasting beaches using a two-phase flow approach. *Adv. Water Res.* **48**, 66–78.

Batchelor, G.K. 1967. *An Introduction to Fluid Dynamics.* Cambridge University Press. 635 pp.

Battjes, J. 1974. Surf similarity. *Proc. 14th Int. Coastal Eng. Conf.* Copenhagen. 466–480.

Bokhove, O. and Peregrine, D.H. 1998. Vorticity and surf zone currents. *Proc. 26th Int. Coastal Eng. Conf.* Copenhagen. 745–758.

Bokhove, O., Zwart, V., and Haveman, M.J., 2010. *Fluid Fascinations.* Stichting Qua Art Qua Science, University of Twente, The Netherlands. The Hele-Shaw experiment was shown at a public lecture of O.B. and Valerie Zwart on 17-01-2010, and built by O.B. and W.Z. in 2x12hrs in the prior weekend, http://eprints.eemcs.utwente.nl/17393/

Calantoni, J. Puleo, J.A., and Holland, K.T. 2006. Simulation of sediment motions using a discrete particle model in the inner surf and swash-zones. *Cont. Shelf Res. 26*, 1987–2001.

Cooker, M. 2010. A commemoration of Howell Peregrine 2007–2010. *J. Eng. Math.* **67**, 1–9.

Deen, N.G., Kriebitzsch, S.H.L., Hoef, M.A. van der, and Kuipers, J.A.M. 2012. Direct numerical simulation of flow and heat transfer in dense fluid-particle systems. *Chemical Eng. Science* **81**, 329–344.

Dumbser, M. 2011. A simple two-phase method for the simulation of complex free surface flows. *Comp. Methods Applied. Mech. Eng.* **200**, 9–12.

Gagarina, E., Ambati, V.R., Van der Vegt, J.J.W., and Bokhove O. 2014. Variational space-time (dis)continuous Galerkin method for nonlinear free surface waves. *J. Comp. Phys.* **275**, 459–483.

Garnier, R., Dodd, N., Falquez, A., and Calvete, D. 2010. Mechanisms controlling crescentic bar amplitude. *J. Geophys. Res.* **115**, F02007.

Hele-Shaw, H.S. 1898. The flow of water. *Nature* **58**. 520–520.

Helluy, P., Golay, F., Caltagirone, J.-P., Lubin, P., Stéphane Vincent, S., Drevard, D., Marcer, R., Philippe Fraunié, Seguin, N., Grilli, S., Lesage, A.-C., and Dervieux, A. 2005. Numerical simulations of wave-breaking. *ESAIM: Math. Modelling Numerical Analysis* **39-2**, 591–607.

Horn, van der, A.J. 2012. Beach Evolution and Wave Dynamics in a Hele-Shaw Geometry. M.Sc. Thesis, Department of Physics, University of Twente.

Lachaume, C., Biausser, B., Grilli, S.T., Fraunie, P., and Guignard, S. 2003. Modeling of breaking and post-breaking waves on slopes by coupling of BEM and VOF methods. In Proc. 13th Offshore and Polar Engng. Conf. (ISOPE03, Honolulu, USA, May 2003), 353-359.

Lamb, H. 1993. Hydrodynamics. Cambridge University Press. 738 pp.

Lee, A.T., Ramos, E., and Swinney, H.L. 2007. Sedimenting sphere in a variable-gap Hele-Shaw cell. *J. Fluid Mech.* **586**, 449–464.

McCall, R.T., van Thiel de Vries, J.S.M., Plant, N.G., van Dongeren, A.R., Roelvink, J.A., Thompson, D.M., and Reniers, A.J.H.M. 2010. Two-dimensional time dependent hurricane overwash and erosion modeling at Rosa Island. *Coastal. Eng.* **57**, 668–683.

Miles, J. 1977. On Hamilton's principle for surface waves. *J. Fluid. Mech.* **27**, 395–397.

Operational models 2014. Delft3D. Software on morphology by Deltares: http://www.deltaressystems.com Open Telemac-Mascaret: http://www.opentelemac.org/ XBeach: http://oss.deltares.nl/web/xbeach/

Pedlosky, J. 1987. *Geophysical Fluid Dynamics*. Springer. 701 pp.

Peregrine, D.H. 1983. Breaking waves on beaches. *Ann. Rev. Fluid Mech.* **15**, 149–178.

Plouraboué, F. and Hinch, E.J., 2002. Kelvin-Helmholtz instaility on a Hele-Shaw cell. Phys. Fluids **14**, 922–929.

Powell, K.A. 1990. Predicting short term profile response for shingle beaches. HR Wallingford. Online Report.

Rajchenbach, J. Lerouz, A., and Clamond, D. 2011. New standing solitary waves. *Phys. Rev. Lett.* **107**, 024502.

Roelvink, D., Reniers, A., van Dongeren, A., van Thiel de Vries, J., McCall, R., and Lescinkski, J. 2009. Modelling storm impacts on beaches, dunes and barrier islands. *Coastal Eng.* **56**, 1133–1152.

Short, A.D. 2000. *Handbook of Beach and Shore-face Dynamics*. Wiley. 379 pp.

Soulsby, R. 1997. *Dynamics of Marine Sands.* In: HR Wallingford. Thomas Telford. 249 pp.

Thornton, A.R., Gray, J.M.N.T, and Hogg, A.J. 2006. Three-Phase Model of Segregation in Granular Avalanche Flows. *J. Fluid Mech.* **550**, 1–25.

Thornton, A.R., Van der Horn, A.J., Gagarina, E., Zweers, W., Van der Meer, D., and Bokhove, O. 2014. Hele-Shaw beach creation by breaking waves: a mathematics-inspired experiment. *J. Environmental Fluid Dynamics* **14**, 1123–1145.

Vega, J.M., Knobloch E., and Martel, C. 2001. Nearly inviscid Faraday waves in annular containers of moderately large aspect ratio. *Physica D* **154**, 313–336.

Vella, D. and Mahadevan, L. 2005. The 'Cheerios Effect'. *American J. Physics* **73**, 817–825.

Williams, J.J., De Algria-Arzburu A.R., McCall, R.T., and Van Dongeren, A. 2012. Modelling gravel barrier profile response to combined waves and tides using XBeach: laboratory and field results. *Coast. Eng.* **63**, 62–80.

Wilson, S.K. and Duffy, B.R. 1998. On lubrication with comparable viscous and inertia forces. *Q.J. Mech. Appl. Math.* **51**, 105–124.